International Journal for Computational Methods in Engineering Science and Mechanics, 15:390–400, 2014

ISSN: 1550-2287 print / 1550-2295 online
DOI: 10.1080/15502287.2014.915253

Taylor & Francis
Taylor & Francis Group

Finite Element Simulation of Two-Dimensional Pulsatile Blood Flow Through a Stenosed Artery in the Presence of External Magnetic Field

Haleh Alimohamadi[1] and Mohsen Imani[2]

[1]*Department of Mechanical Engineering, College of Engineering, University of Tehran, Tehran, Iran*
[2]*Department of Electrical and Computer Engineering, College of Engineering, University of Tehran, Tehran, Iran*

This paper introduces the impact of external magnetic field on blood flow patterns in a stenosis artery. Considering the fatty deposited lump, arterial walls as porous media, and pulsatile inflow base on human-heart-beating rate closes our model to the actual stenosis blood artery. In this study, by solving transient fluid dynamic equations in coupled porous and free media, the velocity, temperature, and shear stress distribution along the lump are investigated. The results show that applying 10^5 magnetic field intensity (Mn_F) creates two vortexes on the lumps' edges and 15X (16.6X) higher shear stress (temperature) in the stenosis region.

Keywords Blood flow, Biomagnetic fluid, Stenosis artery, Heat transfer, Porous media, Magnetization and Lorentz forces

1. INTRODUCTION

Currently, cardiovascular diseases, especially stenosis, are very prevalent and take the lives of many people. This common disease occurs by backlogging macromolecules on the arterial walls and atherosclerotic plaques' formation by the passage of the time. These plaques block the normal path of blood flow, make it narrower and, in critical conditions, close it completely. Biological research shows that these macromolecules are mostly made from fatty material and are vulnerable to high temperature and shear stress, so dissolving them by increasing heat transfer rate or exerting higher viscous forces through applying external magnetic field is a safe and new bioengineering-suggested remedy. Natural blood has an innate, slight magnetization feature and in order to increase this characteristic, additional injected ferro-nanoparticles have recently been used. These particles increase blood magnetization and are mostly organic solvents which can act as solutes. The solution of these nanoparticles in natural and industrial fluids have wide application in bioengineering [1, 2], micro-electrical and mechanical structure [3], cardiovascular and articulate treatments [4, 5], and two-phase flow [6]. During the last few decades, numerous investigations have been done in this new field of biomechanics. Stangeby and Ethier [7] worked out a coupling model of Navier-Stokes and Brinkman equations in free and porous media. The dynamic expression for heat and mass transfer in stenosis artery is introduced in [8]. In [9], the velocity and temperature distribution of biofluid flow under the influence of an external magnetic field are discussed. The latter article modeled the artery as a uniform tub with solid and impenetrable walls. In [10], different models of macro blood flow were coupled with various areas and types of stenosis. The time-dependent heat transfer of two-dimensional blood flow is discussed in [11]; however, this article neglected the porous assumption for arterial walls. The effects of permeability, magnetic field, and body acceleration on blood flow passing through a porous media are brought up in [12], and the analytical solution of stationary non-Newtonian blood flow in porous media at the present of magnetic field is investigated in [13]. The innovation of this article lies in solving transient fluid dynamics equations of blood flow through stenosis geometry taking into account the non-Newtonian viscosity of blood and both magnetization and Lorentz forces. In this study, according to a real heart-beating rate, the time-dependent inlet velocity alters and the impact of the magnetic field on different heart cycles is described. In Part 2, the assumed geometry for a stenosis vessel in addition to the governing equations of fluid flow under the action of magnetic field is discussed. Part 3 is developed to

Address correspondence to Mohsen Imani, Room 401, School of Electrical and Computer Engineering, University College of Engineering, University of Tehran, P.O. Box 14395-515, North Kargar St., Tehran, Iran. E-mail: m.imani1386@gmail.com

Color versions of one or more of the figures in the article can be found online at www.tandfonline.com/ucme.

TABLE 1
Constant value

Parameters	Numerical value	Parameters	Numerical value
ρ	$1050\, kg.m^{-3}$	Ec	8.7×10^{-6}
η	$3.2 \times 10^{-3}\, kg.m^{-1}.s^{-1}$	α	$1.22 \times 10^{-7}\, m^2.s^{-1}$
Re	0.04	k	$1.832 \times 10^{-3}\ Joule.^0K^{-1}m^{-1}s^{-1}$
T_1	$300\,^0K$	Mn_F	$[10^5{:}5{\times}10^5]$
δT	$30\,^0K$	Mn_M	150
Pr	24.95	Da	40-400-4000
C_p	$14.65J.(Kg.K)^{-1}$	χ_0	0.06
μ_0	$4\pi \times 10^{-7}$	β	$5.6{\times}10^{-3}\ K^{-1}$
η_0	$35 \times 10^{-3}\ kg.m^{-1}.s^{-1}$	n	0.6

present the dimensionless equations and boundary conditions and, finally, the simulation results and conclusion are outlined in sections 4 and 5, respectively.

2. ARTERY MODEL AND MATHEMATICAL FORMULATION

2.1 Stenosis Artery Model

In this article, we consider a viscous, laminar, incompressible, transient and two-dimensional blood flow between two porous plates. Uniform flow enters the domain and, in the middle of the vessel ($L_f < x < L_f + L_s$), one porous lump on the lower plate blocks the normal blood flow path. Both up and down vessel walls are assumed at the constant temperature and the length and height of the artery are shown by L and h, respectively. The flow is subjected to an external magnetic force producing an infinite current plate along the z axis. The non-symmetric stenosis blood artery is shown in Fig. 1 and presumed as below function [14]:

$$\frac{y}{h} = \begin{cases} 0.7 - \frac{3d}{2hL^4}[11(x-L_f)L_s^3 - 47(x-L_f)^2L_s^2 \\ +72(x-L_f)^3L_s - 36(x-L_f)^4] & L_f \le x \le L_s + L_f. \\ 1 \qquad otherwise \end{cases}$$

The porous assumption for arterial walls and the fatty deposited plaque is conforming to actual behavior of our blood artery. As depicted in Fig. 1, 15% total artery thickness is assigned to each porous arterial wall and "d" is the maximum height of stenosis, which depends on the disease progression, and its increment can create a critical condition for patients.

2.2 Heat Transfer and Fluid Flow Equations

Under the action of an external magnetic field, two kinds of forces affect the blood flow. One of them is magnetization force, which appears due to magnetic field gradient, and the second is the Lorentz force, which should be taken into account because of the high electrical conductivity of blood flow and ferronanoparticles' solution. The governing equations on the non-Newtonian flow under the action of the external magnetic field are described as below:

Continuity equation:

$$\nabla.\vec{V}^* = 0 \tag{1}$$

Momentum equation [15]:

$$\rho\frac{D\vec{V}^*}{Dt^*} = -\nabla p^* + \eta\nabla^2\vec{V}^* + J^* \times B^* + \mu_0 M^*\nabla H^* \tag{2}$$

Energy equation [15]:

$$\rho C_p\frac{DT^*}{Dt^*} + \mu_0 T^*\frac{\partial M^*}{\partial T^*}\frac{DH^*}{Dt^*} - \frac{J^*.J^*}{\sigma} = k\nabla^2 T^* + \eta\phi^* \tag{3}$$

where $\vec{V}^* = (u^*, v^*)$is the two-dimensional velocity field, $\frac{D}{Dt^*} = \frac{\partial}{\partial t^*} + V^*\nabla$ is the material derivative, $\nabla = (\frac{\partial}{\partial x^*}, \frac{\partial}{\partial y^*})$ is the gradient operator, $\nabla^2 = \nabla.\nabla = (\frac{\partial^2}{\partial x^{*2}}, \frac{\partial^2}{\partial y^{*2}})$ is the Laplacian operator, ρ is the fluid density, P is the pressure, η is the dynamic viscosity, μ_0 is the magnetic permeability of vacuum, M^* is the magnetization, H^* is the magnetic field intensity, B^* is the magnetic induction where $B^* = \mu_0(M^* + H^*)$, σ is the electrical conductivity of the fluid, J^* is the density of the electrical current, T^* is the temperature, k is the thermal conductivity, C_p is the specific heat at constant pressure, and φ^* is the dissipation factor. For the two-dimensional problem, it is written as:

$$\phi^* = 2\left(\frac{\partial u^*}{\partial x^*}\right)^2 + 2\left(\frac{\partial v^*}{\partial y^*}\right)^2 + \left(\frac{\partial v^*}{\partial x^*} + \frac{\partial u^*}{\partial x^*}\right)^2 \tag{4}$$

The $\mu_0 M^*\nabla H^*$ and $J^*{\times}B^*$ terms in the momentum equation demonstrate the magnetization and Lorentz forces, respectively, which appear because of Magneto Hydro Dynamic (MHD) and Ferro Hydro Dynamic (FHD) effects. In this article, the power law model is used for modeling non-Newtonian blood flow viscosity [16]:

$$\eta = \eta_0\,|\dot{\gamma}|^n \tag{5}$$

η_0 and n are constant parameters and their values are cited in Table 1.

TABLE 2
Time variation of Nusselt number in different magnetic fields with $Mn_M = 10^2$

	Time Step			
Mn_F	*2*	*4*	*6*	*8*
0	0.756	0.089	0.011	−0.001
10^5	0.692	0.059	−0.012	−0.023
2×10^5	0.609	−0.006	−0.070	−0.080
3×10^5	0.504	−0.090	−0.147	−0.155
4×10^5	0.389	−0.179	−0.232	−0.237
5×10^5	0.282	−0.269	−0.317	−0.322

2.3 The Brinkman Equations for the Porous Media Flow

As was mentioned before, the artery walls and the lump are considered as porous media in this study. For simulating the combination of porous and free flow, the Brinkman equations have great accuracy. These equations for the porous regions are expressed as:

Continuity equation:

$$\nabla.\vec{V}_p^* = 0 \tag{6}$$

Momentum equation:

$$\frac{\rho}{\varepsilon_p}\frac{\delta\vec{V}_p^*}{\delta t^*} = -\nabla p^* + \frac{\eta}{\varepsilon_p}\nabla^2\vec{V}_p^* - \frac{\eta}{k_{br}}\vec{V}_p^* + J^*\times B^* + \mu_0 M^*\nabla H^* \tag{7}$$

where $\overrightarrow{V_p^*} = (u_p^*, v_p^*)$,$\varepsilon_p$ and k_{br} are velocity field, porosity, and permeability of the porous regions. The magnetization and Lorentz force are exerted to the porous regions as well. After obtaining the velocity field in the porous regions, the temperature distribution in these domains is calculated by Eq. (3).

2.4 Magnetic Formula

For controlling blood flow in the artery, the magnetic field as an external force is applied to the stenosis region. This magnetization is created by a current plate along the z axis and below the stenosis region.

TABLE 3
Effect of porosity value on maximum temperature with different percent of artery stenosis and $Mn_F = 10^5$, $Mn_M = 10^2$ at time = 1

	d/h			
Darcy Number	0.1	0.15	0.2	0.25
40	10.43	10.40	10.38	10.36
400	10.25	10.24	10.21	10.19
4000	10.23	10.21	10.19	10.17

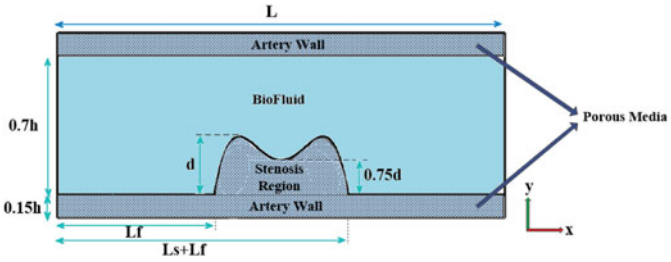

FIG. 1. Modeled stenosis artery.

According to Maxwell's law, the external magnetic field is explained based on the equations below:

$$\nabla\times H^* = J^* = \sigma(\vec{V}^*\times B^*) \tag{8}$$

$$\nabla.B^* = \nabla.(H^* + M^*) = 0 \tag{9}$$

The magnetic field intensity components (H_x^*, H_y^*) of a current plate are given by the expressions below:

$$H_y^* = -\frac{H_0}{2}\left[Ln\left(\frac{(x^*-x_2^*)^2+(y^*-y_0^*)^2}{(x^*-x_1^*)^2+(y^*-y_0^*)^2}\right)\right] \tag{10}$$

$$H_x^* = H_0\left[\tan^{-1}\left(\frac{(x^*-x_2^*)}{y^*-y_0^*}\right) - \tan^{-1}\left(\frac{(x^*-x_1^*)}{y^*-y_0^*}\right)\right] \tag{11}$$

$$H^* = \sqrt{H_y^{*2} + {H_x}^{*2}} \tag{12}$$

H_0 is the magnetic field strength which depends on the applied magnetics induction ($B^* = \mu 0\,(H^*+M^*)$) and x^*_1, x^*_2, y^*_0 are the positions of the horizontal plate, as shown in Fig. 2. The magnetic field and magnetization force components in the entire 2D space of the artery are illustrated in Fig. 3. As described earlier, magnetization force consists of multiplying magnetic field and its gradient in different points of space. Thus, magnetic force is severely high at the edges of the plate where the magnetic field starts and stops. This force affects blood flow and diverts it from direct motion. The x-component of this force attempts to stop the fluid motion and return it backward, while the y-component drags ferroparticles upwards. These two forces can produce circulating flow near the stenosis region, which is the focus of this article.

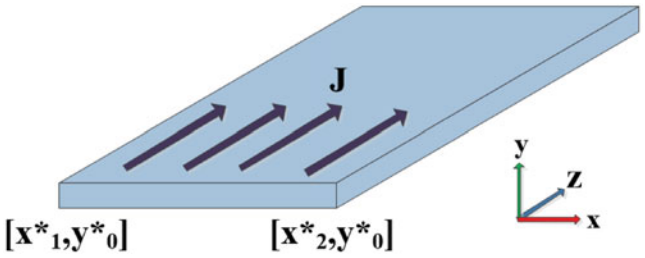

FIG. 2. The plate with current passes through the z direction.

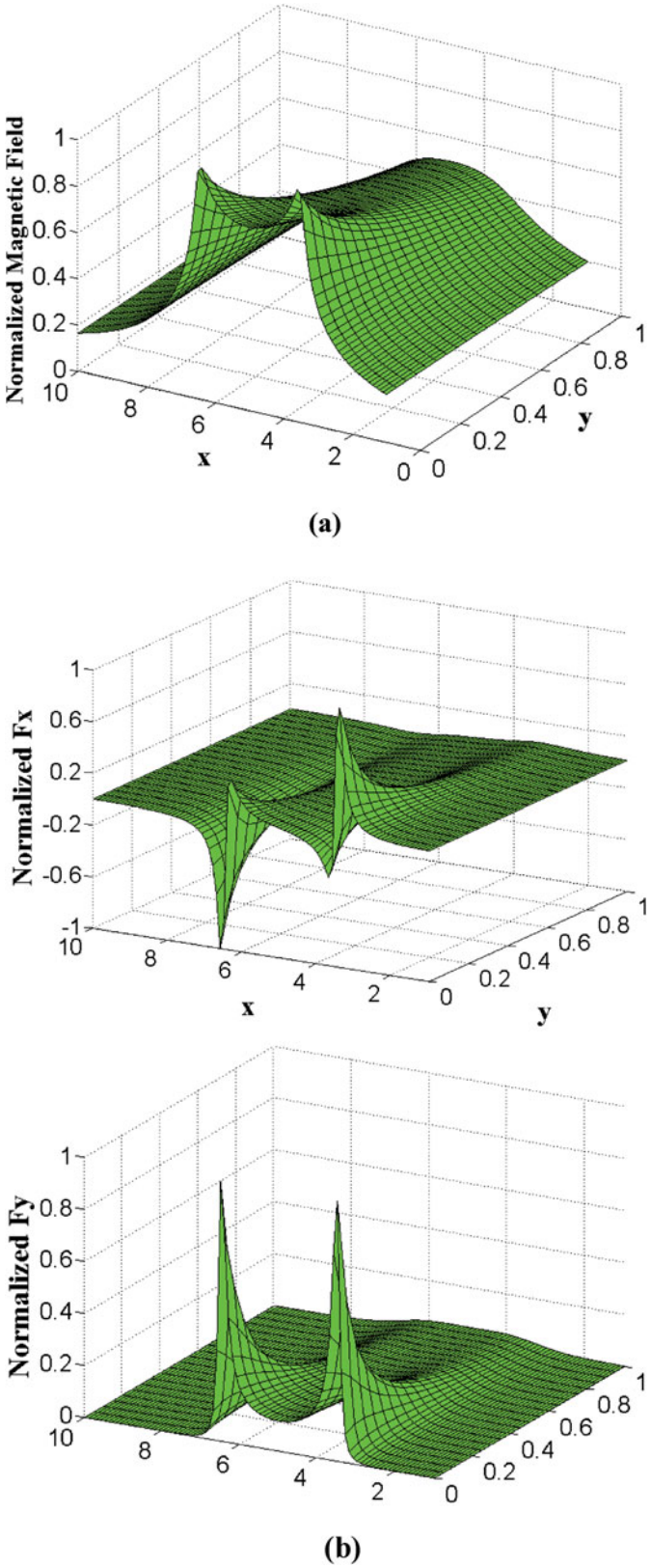

FIG. 3. (a) Normalized total magnetic field intensity; (b) normalized x and y magnetization force components produced by a fixed current plate.

2.5 Magnetization Equation

Magnetization property (M) is a feature of biofluid, which determines the impression of magnetic field on the flow. Various equations for magnetization property have been introduced; in this article, the linear formula that relates the magnetization to magnetic field strength and temperature is used [17]:

$$M^* = \chi_m^* H^* \tag{13}$$

χ_m^* is the magnetic susceptibility and varies with temperature:

$$\chi_m^* = \frac{\chi_0}{1 + \beta(T^* - T_0)} \tag{14}$$

χ_0, βandT_0 are constant parameters that are obtained by experimental data [17].

3. TRANSFORMATION OF EQUATIONS

In order to solve the coupled systems of equations, the following non-dimensional variables are introduced:

$$t = \frac{\alpha}{h^2} t^* \; x = \frac{x^*}{h} \; y = \frac{y^*}{h} \; u = \frac{u^*}{u_r} \; v = \frac{v^*}{u_r} \; p = \frac{p^*}{\rho u_r^2} \; H = \frac{H^*}{H_0} \; T = \frac{T^*}{\delta T} \tag{15}$$

where $\alpha = \frac{\mathrm{K}}{\rho \mathrm{c_p}}$ is the thermal diffusivity of fluid and $u_r = \frac{\alpha}{h}$ is the characteristic velocity.

By substituting these non-dimensional variables into Eqs. (1)–(7) and (14), we have:

In the free flow:

Continuity:

$$\frac{\partial u}{\partial x} + \frac{\partial v}{\partial y} = 0 \tag{16}$$

x-momentum:

$$\frac{\partial u}{\partial t} + u\frac{\partial u}{\partial x} + v\frac{\partial u}{\partial y} = -\frac{\partial p}{\partial x} + \mathrm{Pr} \times |\dot{\gamma}| \left(\frac{\partial^2 u}{\partial x^2} + \frac{\partial^2 u}{\partial y^2} \right) + Mn_F \chi_m H \frac{\partial H}{\partial x} + \frac{Mn_M}{\mathrm{Re}} (\chi_m + 1)^2 (v H_x H_y - u H_y^2) \tag{17}$$

y-momentum:

$$\frac{\partial v}{\partial t} + u\frac{\partial v}{\partial x} + v\frac{\partial v}{\partial y} = -\frac{\partial p}{\partial y} + \mathrm{Pr} \times |\dot{\gamma}| \left(\frac{\partial^2 v}{\partial x^2} + \frac{\partial^2 v}{\partial y^2} \right) + Mn_F \chi_m H \frac{\partial H}{\partial y} + \frac{Mn_M}{\mathrm{Re}} (u H_x H_y - v H_y^2) \tag{18}$$

Also, the energy equation is transformed into:

$$\frac{\partial T}{\partial t} + u\frac{\partial T}{\partial x} + v\frac{\partial T}{\partial y} = \left(\frac{\partial^2 T}{\partial x^2} + \frac{\partial^2 T}{\partial y^2} \right) + Ec \times \mathrm{Pr} \times |\dot{\gamma}| \left(2\left(\frac{\partial u}{\partial x}\right)^2 + 2\left(\frac{\partial v}{\partial y}\right)^2 + \left(\frac{\partial v}{\partial x} + \frac{\partial u}{\partial y}\right)^2 \right)$$

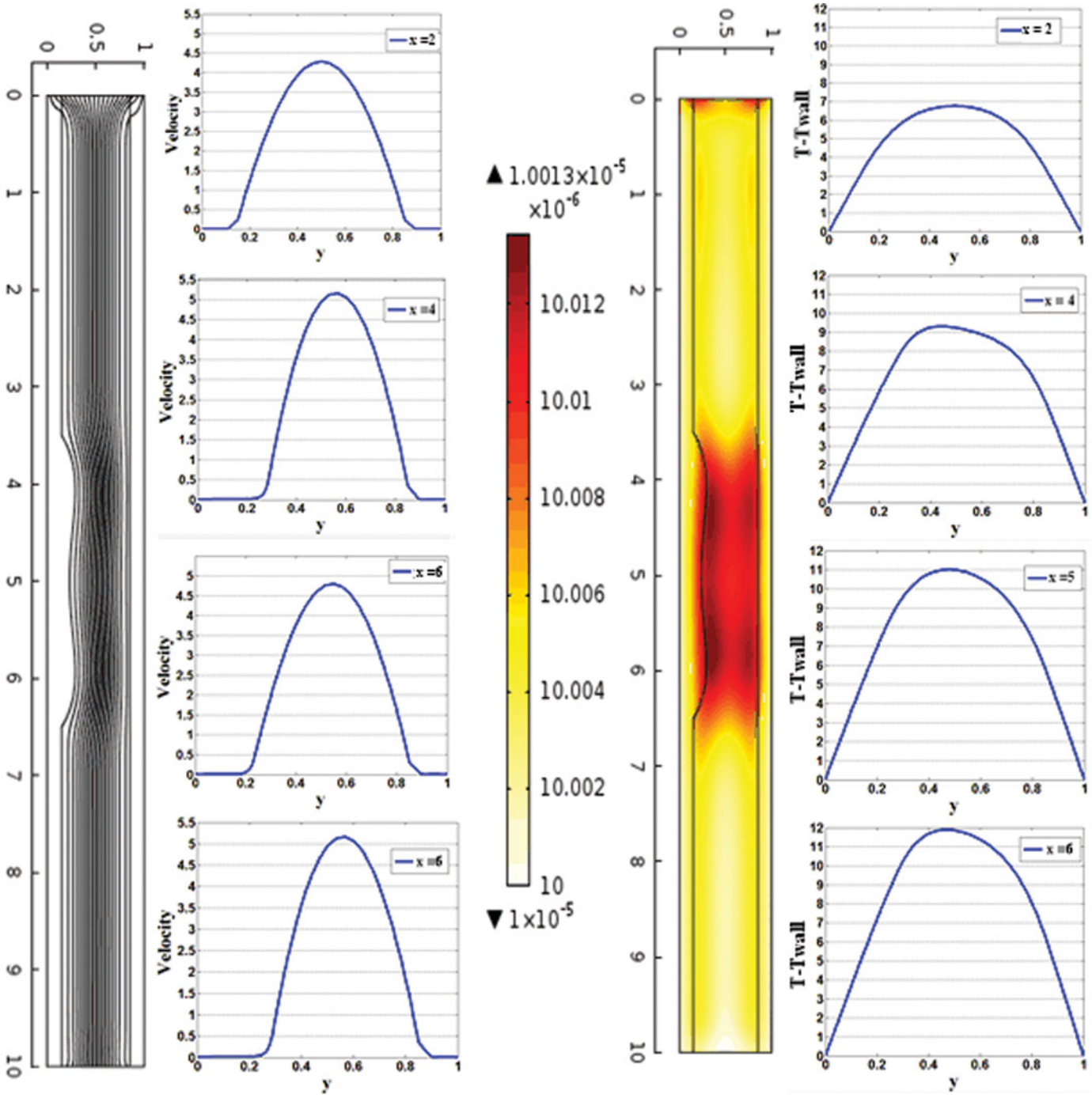

FIG. 4. Stream function and temperature contours with velocity and temperature profiles at time = 1 in different locations.

$$-Mn_F \times Ec \times \frac{\partial \chi}{\partial T} T \times H \left(u \frac{\partial H}{\partial x} + v \frac{\partial H}{\partial y} \right) + \frac{Mn_M}{\mathrm{Re}} \times Ec \times (\chi_m + 1)^2 \times (uH_y - vH_x)^2 \quad (19)$$

For the porous region, the continuity and energy equations are similar to the free flow, but the momentum equation is:

x momentum:

$$\frac{\partial u_p}{\partial t} = -\frac{\partial p}{\partial x} + \mathrm{Pr} \times |\dot{\gamma}| \left(\frac{\partial^2 u_p}{\partial x^2} + \frac{\partial^2 u_p}{\partial y^2} \right) + \mathrm{Pr} \times |\dot{\gamma}| \times Da \times u_p + Mn_F \times \chi_m \times H \frac{\partial H}{\partial x} + \frac{Mn_M}{\mathrm{Re}} (\chi_m + 1)^2 (v_p H_x H_y - u_p H_y^2) \quad (20)$$

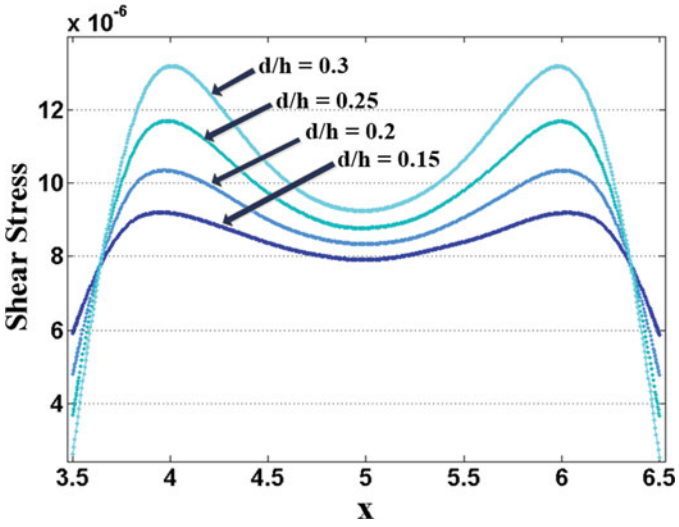

FIG. 5. Shear stress in the stenosis region in different d/h at time = 1.

y momentum:

$$\frac{\partial v_p}{\partial t} + u_p \frac{\partial v_p}{\partial x} + v_p \frac{\partial v_p}{\partial y} = -\frac{\partial p}{\partial y} + \Pr \times |\dot{\gamma}|$$

$$\left(\frac{\partial^2 v_p}{\partial x^2} + \frac{\partial^2 v_p}{\partial y^2}\right) + \Pr \times |\dot{\gamma}| \times Da \times v_p + Mn_F$$

$$\chi_m H \frac{\partial H}{\partial y} + \frac{Mn_M}{\mathrm{Re}}(u H_x H_y - v H_y^2) \tag{21}$$

where

$$\chi_m = \frac{\chi_0}{1 + (\beta \delta T)(T - \frac{T_0}{\delta T})} \tag{22}$$

The non-dimensional parameters which appear in the above equations are:

$$\mathrm{Re} = \frac{h\rho u_r}{\eta} = \frac{\rho\alpha}{\eta} \text{ (Reynolds number)} \tag{23}$$

$$Ec = \frac{u_r^2}{C_p \delta T} = \frac{\alpha^2}{C_p \delta T h^2} \text{ (Eckert number)} \tag{24}$$

$$\Pr = \frac{\eta}{\rho\alpha} \text{ (Prandtl number)} \tag{25}$$

$$Da = \frac{h^2}{k_{br}} \text{(Darcy number)} \tag{26}$$

$$Mn_F = \frac{\mu_0 H_0^2}{\rho u_r^2} = \frac{\mu_0 H_0^2 h^2}{\rho \alpha^2} \text{ (Magnetic number of FHD)} \tag{27}$$

$$Mn_M = \frac{\mu_0^2 H_0^2 h^2 \sigma}{\eta} \text{ (Magnetic number of MHD)} \tag{28}$$

The two magnetic numbers appear because of magnetization and Lorentz forces, and if they are set to zero, the problem reduces to an ordinary flow between two plates with heat transfer.

3.1 Boundary Conditions

In order to solve Eqs. (16)–(21) simultaneously, the non-dimensional boundary conditions below are applied:

- For the upper wall ($y = 1\, and\, 0 < x < 10$), the temperature is constant (T_1) and the velocity is zero (no slip condition);
- For the lower plate ($y = 0\, and\, 0 < x < 10$), the temperature is constant (T_1) and the velocity is zero (no slip condition);
- For outlet ($x = 10\, and\, 0 < y < 1$), the temperature gradient ($\frac{\partial T}{\partial x}$) and the pressure are zero;

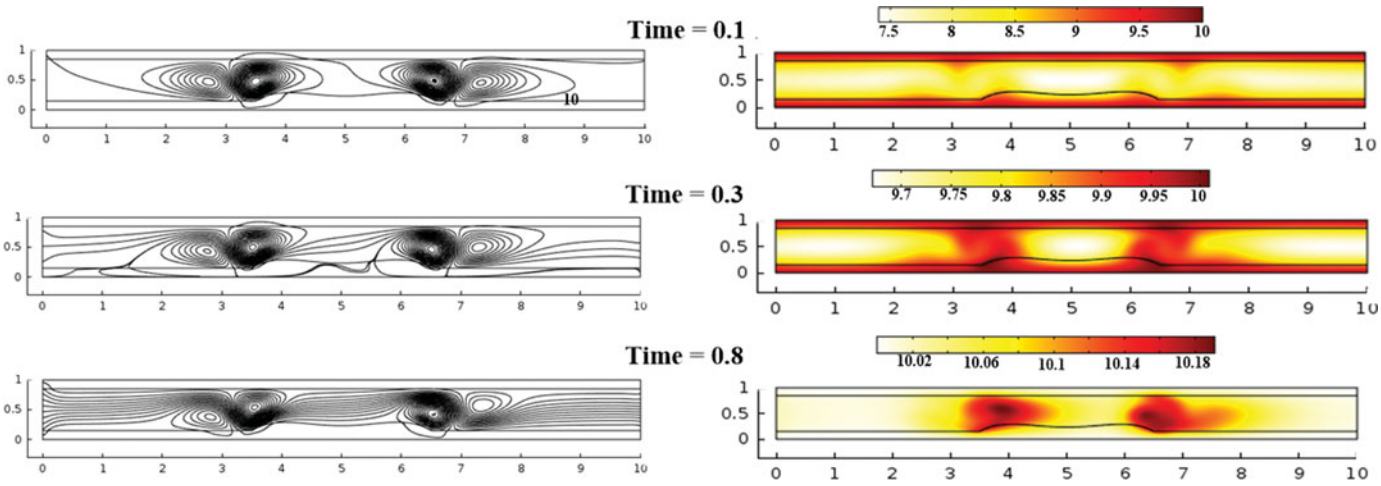

FIG. 6. Streamlines and temperature contours with $\mathrm{Mn_F} = 10^5$ and $\mathrm{Mn_M} = 10^2$ in different time steps.

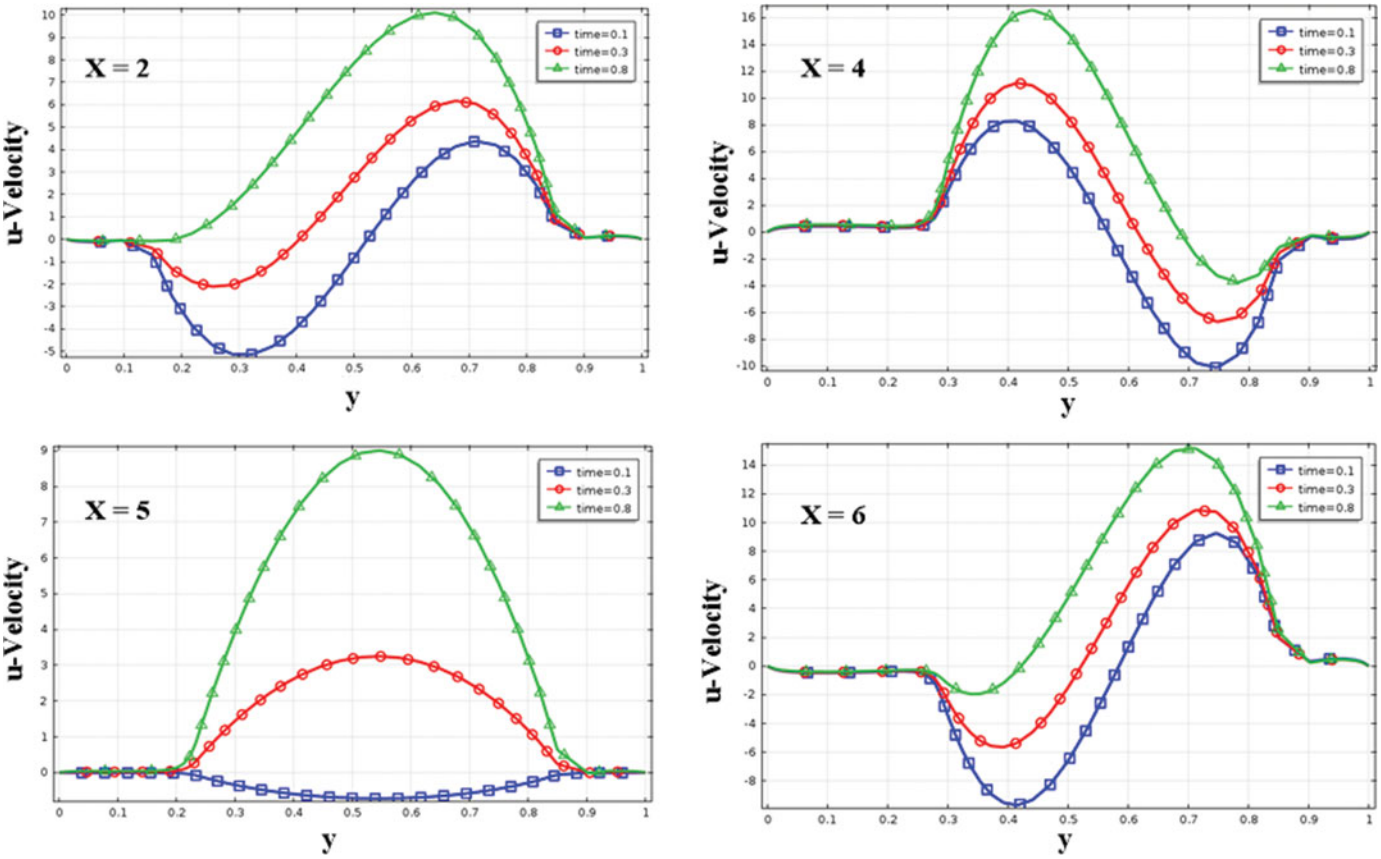

FIG. 7. The time variation of "u" velocity profile for different locations with $Mn_F = 10^5$ and $Mn_M = 10^2$.

- For inlet ($x = 0 and 0 < y < 1$), the temperature is constant (T_1) and the uniform inflow velocity changes with time according to [18];
- For the free-porous interface, it is assumed that velocity is equal in these two regions ($\vec{V_p} = \vec{V}$.). This condition means that the velocity field remains continuous between free and porous media.

4. SIMULATION RESULT

In this article, the current plate is fixed at $x_1 = 3.3$, $x_2 = 6.7$, and $y_0 = -0.1$ in order to encompass the entire critical region and produce the maximum magnetic forces at the starting and ending edges of the lump. The fluid is assumed to have non-Newtonian behavior and its electrical conducting is noticeable. The time-dependent flow in the described geometry is solved with COMSOL 4.3 code using a direct UMFPACK linear system solver. The constant values that are used in this paper are archived in Table 1 [9, 11].

4.1 Flow in Stenosis Artery without Magnetic Force

In order to reach the fully developed flow before and after the stenosis region, the ratio of stenosis length to total length (L_s/L) is assumed to be small enough in this study. Thus, the entry length is too small and the flow soon reaches the fully developed condition, but in the stenosis region, due to a narrowing of the cross-sectional area, the velocity magnitude increases. Fig. 4 shows the non-dimensional velocity and temperature contours with 20% artery stenosis. The dimensionless "u" velocity component and temperature profiles in specific locations along the vessel are shown in this figure. As expected, the flow has fully developed behavior in each cross-section, and the velocity magnitude near the arterial walls (x = 2 graph in Fig. 4) and inside the formed plaque (x = 4, 5, 6 graph in Fig. 4) is extremely low because of the porosity feature of the walls and lump.

In fluid mechanics, the temperature directly relates to the velocity magnitude and the fluid temperature increase if it moves faster. As seen in Fig. 4, the stenosis region has the highest temperature because of stream line contraction and flow acceleration in this area. As the added temperature graphs show, the maximum increment of temperature in the stenosis region is equal to 12mK (x = 6 in Fig. 4).

The dimensionless shear stress distribution on the lump is elucidated in Fig. 5. By reaching to the first throat, the shear stress value jumps severely due to increasing velocity gradient above the lump. The shear stress decreases until the middle of

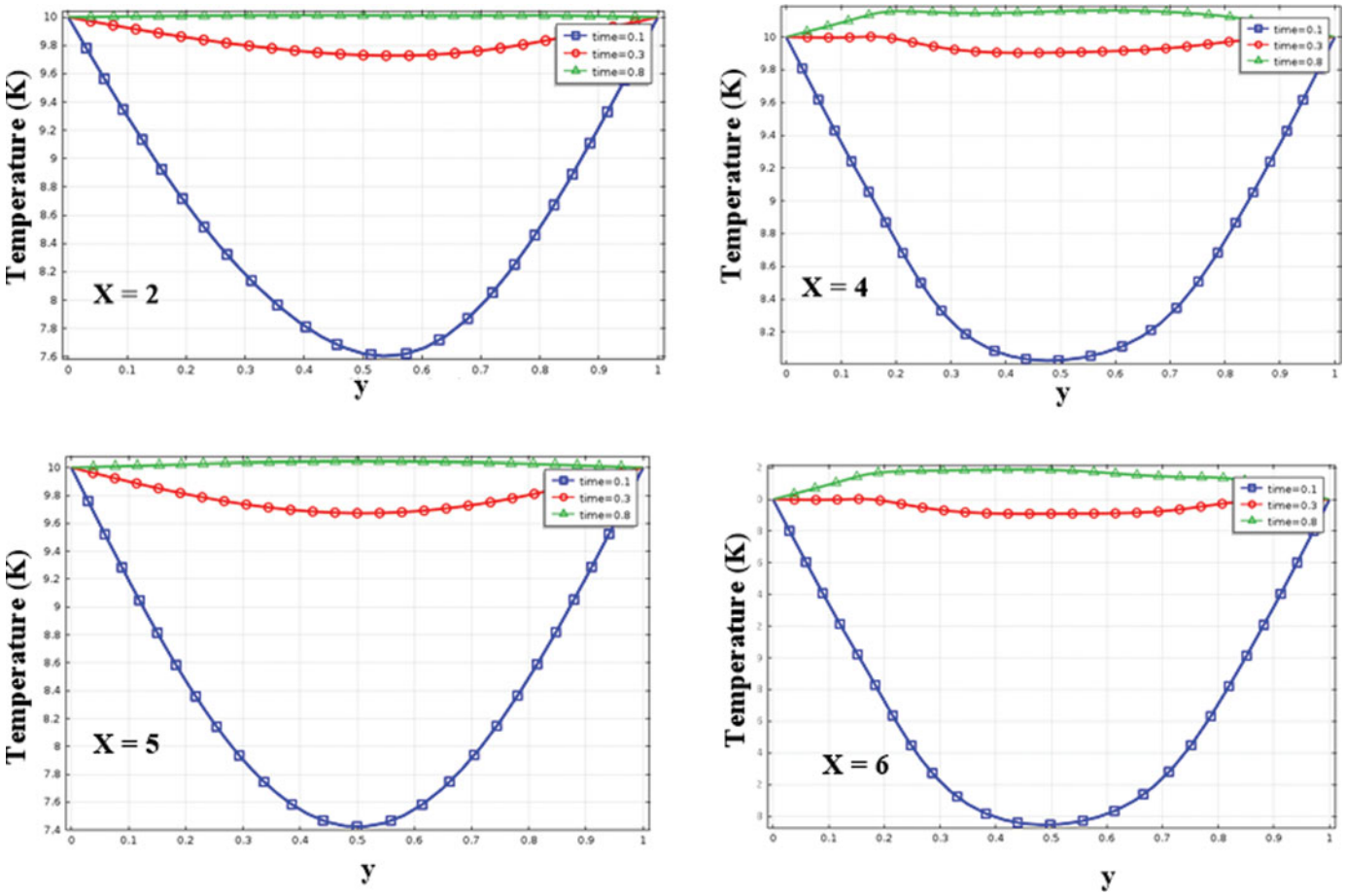

FIG. 8. The time variation of temperature profile in different x-positions with $Mn_F = 10^5$ and $Mn_M = 10^2$.

the lump region; after that, it rises up through the second throat. As depicted in the figure, by increasing the stenosis percent, the lump must tolerate higher shear stress because, with increasing stenosis height, the available cross-sectional area for blood flow becomes narrower and higher velocity gradients are exerted on the lump. The shear stress trend and its increment, by increasing the stenosis percent, coincides with calculated results in the paper [14].

4.2 Time-Dependent Effect of Magnetic Field on Blood Flow

The stream function and temperature contours at the present external magnetic field and at three different time steps (t = 0.1, 0.3, 0.8) are demonstrated in Fig. 6. The primary effect of the exerting magnetic field is the formation of two main vortexes approximately at the edges of the current plate (x = 3.5 and x = 6.6). The first vortex rotates counter-clockwise while the second one revolves in the opposite direction. At t = 0.1, the inlet velocity is negative, so the number of streamlines between the two vortices are much fewer than at other times. With the passage of time, the inlet velocity becomes positive and peaks at t = 0.3 and t = 08; the power of viscosity and inertia forces becomes remarkable and competes with magnetic forces. As the figure at t = 0.8 shows, these two forces partly overcome the magnetic force, increasing the number of streamlines in the channel and weakening the vortices' size and effect.

On the other hand, the temperature contours depict that, with the passage of the time, not only does the maximum temperature go up, but it also focuses on the first and end edges of the lump, where the vortices are created and the flow circulates. Atherosclerotic plaques are usually formed from fatty deposits and can be dissolved in high ambient temperature. In fact, the current plate acts as an external heat term that produces two concentrated heat sources on the lump's edges and can be beneficial for eliminating these fatty plaques. Furthermore, the formed vortices can be useful for targeting drug delivery since the flow circulation creates stagnant flow above the specific area and drug carriers could have more accessible time for activation and absorption.

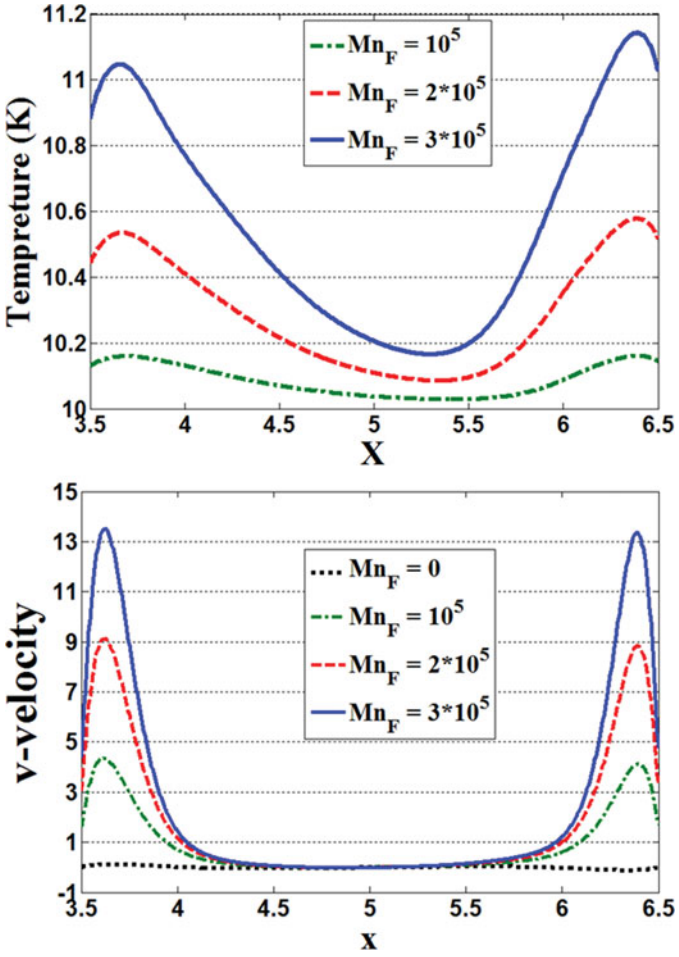

FIG. 9. Temperature and v-velocity profile in the stenosis region with different magnetic field intensity and $Mn_M = 10^2$ at time = 1.

The time variation of dimensionless axial velocity at the external magnetic field and for specific locations is depicted in Fig. 7. The location x = 2 is far from the magnetic plate and the effect of the formed vortices in this region is less than in other areas. As seen, with the passage of time the effect of the magnetic forces declines because the inlet velocity increases and the viscous and inertia forces become prominent such that the velocity profile at t = 0.8 is similar to its parabolic profile without impact of magnetization forces (see Fig. 4). The trend of velocity profiles at x = 4 and x = 6 is reversed since the vortices in these regions rotate in opposite directions. At x = 5, two opposite vortices neutralize each other's impact and the "u" velocity profile in this location resembles the figure with its non-magnetization effect (see Fig. 4).

Increasing the temperature in respect to time and in different locations is shown in Fig. 8. As the trend of this figure elucidates, with the passage of time the fluid temperature increases such that at x = 6, where the second vortex is formed, this increment

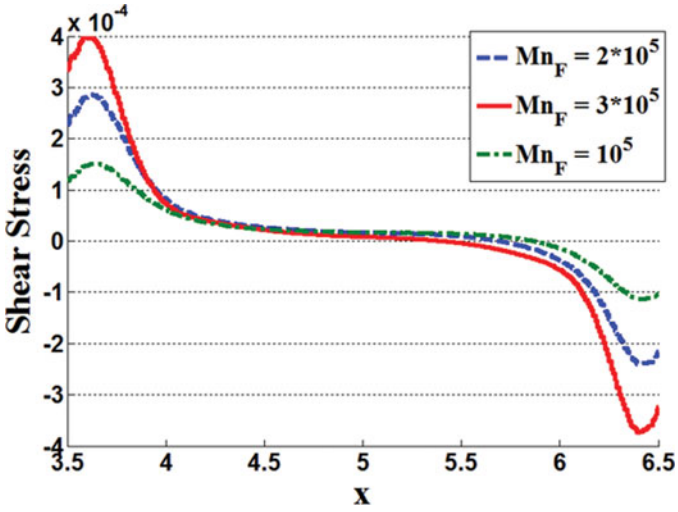

FIG. 10. Shear stress distribution in the stenosis region with different values of magnetic field intensity and $Mn_M = 10^2$ at time = 1.

is maximized and the fluid temperature is 0.2 K higher than the walls.

4.3 Effect of Magnetic Field Intensity on Fluid Flow

The magnetic field intensity has a direct impact on the penetration velocity, temperature, vortex size, and shear stress. The effect of this parameter on the temperature and vertical velocity along the stenosis region is demonstrated in Fig. 9. As shown in this figure, by doubling and tripling the magnetic field intensity from 10^5, the maximum velocity (temperature) increases about 2.25X and 3.4X (1.02X and 10.1X), respectively.

By strengthening the magnetic field, the bigger vortices influence a wider area and higher velocity gradient applied stronger shear stress to the lump. By applying the magnetic field with two (three) times stronger from 10^5, the maximum shear stress will become 2X (2.8X) higher in the stenosis region.

Our simulation shows, at first time steps, that the blood temperature is lower than the arterial walls and heat transfers from the walls to the fluid, but with time, the blood becomes warmer and the heat transfer direction is reversed.

This occurrence is elucidated in Table 2, such that the Nusselt number varies from a positive value to a negative value through one heart cycle. The heat transfer rate speeds up by strengthening magnetic field intensity and bigger vortices formation, and as the table shows, at t = 8 with a five-times increase in magnetic field intensity from 10^5 to 5×10^5, the value of the Nusselt number goes up about 13.5X. Generally, the results of this section indicate that by applying a more powerful external magnetic field, the magnitude of temperature, penetration velocity, and shear stress on the stenosis region go up remarkably and the high value of these parameters can be useful for cutting, corrosion, and dissolving the fatty lump from the vessel's wall.

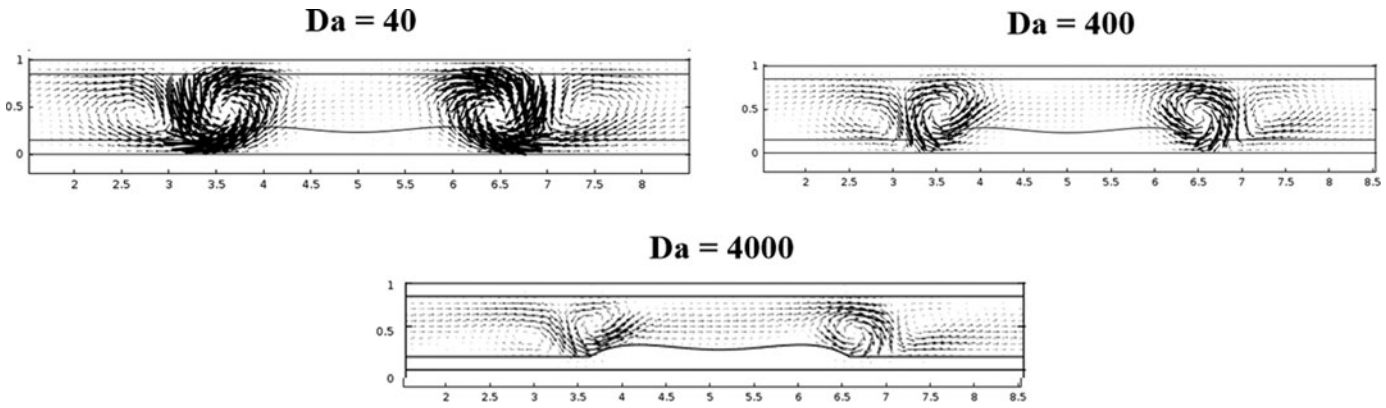

FIG. 11. Velocity arrows in the artery with different porosity values of walls and stenosis region with $Mn_F = 10^5$ and $Mn_M = 10^2$ at time = 1.

4.4 Effect of Porosity on Magneto-Therapy Performance

The porous permeability effect on the vortex power and penetration velocity in the stenosis area is illustrated in Fig. 11 and Fig. 12, respectively. Based on Fig. 11, a decreasing Darcy number value causes bigger and stronger vortices to form in the stenosis region, reducing the Darcy number about two orders of magnitude and creating a six-times-higher vertical velocity and penetration flow into the fatty lump (see Fig. 12). These results make it clear that stenosis disease has better treatment under a magneto-therapy process in the preliminary level because the fatty lumps are more penetrable (lower Darcy number), and even one weak external magnetic field can affect them.

Table 3 demonstrates the maximum blood temperature for different porosity factors and stenosis heights. Increasing both porosity and stenosis height parameters makes the magneto-therapy less efficient because, by increasing the value of the Darcy number, the porous regions become more rigid, hardly resisting against the flow passage, and the available cross-sectional area for blood flow declines. Thus, based on continuity law, the velocity magnitude and, consequently, the inertia and viscosity forces become powerful enough to attenuate the external magnetic field effect such that, by increasing the value of the Darcy number about two orders of magnitude, the maximum blood temperature declines at least 2%. In addition, stenosis progression has the same negative effect on the magneto-therapy effectiveness, as a lower temperature is produced on the fatty lump, and obtaining higher temperature on the stenosis region can help to dissolve the lump tissue faster and more easily. Hence, according to this table, using magnetic field and magneto therapy can be more effective for patients who have a low percent of stenosis and whose blood vessels or formed lumps on their arterial walls are not yet rigid.

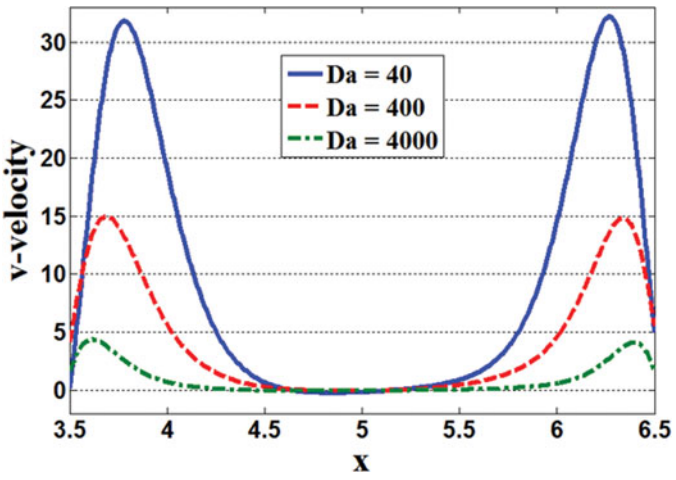

FIG. 12. V-velocity on the stenosis region with different Darcy numbers and $Mn_F = 10^5$ and $Mn_M = 10^2$ at time = 1.

5. CONCLUSION

In this article, a transient study of magnetic field effect on a stenosed artery, considering the arterial walls and atherosclerotic plaque as a porous media, is investigated. The blood viscosity treats as a non-Newtonian fluid and an infinite current plate is fixed under the stenosis region to produce two vortices on the lump's edges. These vortices act as additional heat sources, making the lump warmer and creating a suitable condition for dissolving it. The applied external magnetic field increases shear stress value on the stenosis region, which can rub out and wash away the fatty deposited plaques. In addition, the simulation results show that, for a magneto-therapy process, a lower porous lump is more appropriate, since bigger vortices can create higher temperature and penetration velocity along the target site.

REFERENCES

1. M. Pinho, B. Brouard, J.-M. Génevaux, N. Dauchez, O. Volkova, H. Mézière, and P. Collas, Investigation Into Ferrofluid Magnetoviscous Effects Under An Oscillating Shear Flow, J. Mag. and Mag. Mat., vol. 323, pp. 2386–2390, 2011.
2. A. Nacev, C. Beni, O. Bruno, and B. Shapiro, The Behaviors Of Ferromagnetic Nano-Particles In And Around Blood Vessels Under Applied Magnetic Fields, J. Mag. and Mag. Mat., vol. 323, pp. 651–668, 2011.
3. S. Pal, A. Datta, S. Sen, A. Mukhopdhyay, K. Bandopadhyay, and R. Ganguly, Characterization Of A Ferrofluid-Based Thermomagnetic Pump For

Microfluidic Applications, J. Mag. and Mag. Mat., vol. 323, pp. 2701–2709, 2011.
4. H. Alimohamadi and M. Imani, Computational Analysis Of Synovial Fluid In Actual Three-Dimensional Modeling Of Human Knee Joint Under The Action Of Magnetic Field, Int. J. Energy and Tech., vol. 4, pp. 96–103, 2013.
5. H. Alimohamadi, M. Imani, and M. Shojaee-Zadeh, Computational Analysis Of Pulsatile Biofluid In Locally Expanded Vessel Under The Action Of Magnetic Field, Adv. In App. Sci. Res. J., vol. 5, pp. 1–8, 2013.
6. H. Aminfar, M. Mohammadpourfard, and F. Mohseni, Two-Phase Mixture Model Simulation Of The Hydro-Thermal Behavior Of An Electrical Conductive Ferrofluid In The Presence Of Magnetic Fields, J. Mag. and Mag. Mat., vol. 324, pp. 830–842, 2012.
7. D.K. Stangeby and C.R. Ethier, Computational Analysis Of Coupled Blood-Wall Arterial LDL Transport, J. Biomech. Eng., vol. 124, pp. 1–8, 2002.
8. S. Chakravarty and S. Sen, Dynamic Response Of Heat And Mass Transfer In Blood Flow Through Stenosed Bifurcated Arteries, Korea-Aust. Rheol. J., vol. 17, pp. 47–62, 2005.
9. E. Tzirtzilakis and V. Loukopoulos, Biofluid Flow In A Channel Under The Action Of A Uniform Localized Magnetic Field, Comp. Mech., vol. 36, pp. 360–374, 2005.
10. L. Ai and K. Vafai, A Coupling Model For Macromolecule Transport In A Stenosed Arterial Wall, Int. J. Heat and Mass Trans., vol. 49, pp. 1568–1591, 2006.
11. T. Strek and H. Jopek, Computer Simulation Of Heat Transfer Through A Ferrofluid, Physica Status Solidi (B), vol. 244, pp. 1027–1037, 2007.
12. V. Rathod and S. Tanveer, Pulsatile Flow Of Couple Stress Fluid Through A Porous Medium With Periodic Body Acceleration And Magnetic Field, Bull. Malays. Math. Sci. Soc. (2), vol. 32, pp. 245–259, 2009.
13. J. Singh and R. Rathee, Analytical Solution Of Two-Dimensional Model Of Blood Flow With Variable Viscosity Through An Indented Artery Due To LDL Effect In The Presence Of Magnetic Field, Int. J. Phys. Sci., vol. 5, pp. 1857–1868, 2010.
14. S. Chakravarty and P. Mandal, Mathematical Modelling Of Blood Flow Through An Overlapping Arterial Stenosis, Math. and Comp. Mod., vol. 19, pp. 59–70, 1994.
15. E. Tzirtzilakis, A Mathematical Model For Blood Flow In Magnetic Field, Physics Of Fluids, vol. 17, pp. 1–15, 2005.
16. S.-B. Wang, L. Du, C.-X. Sun, S. Lin, and Y. Yang, Reciprocity Property Of Magneto-Optical Rotation Effect Of Ferrofluid Exposed To The Longitudinal Magnetic Field, High Voltage Eng., vol. 8, pp. 1–8, 2010.
17. F. Scarpa and F. Smith, Passive And MR Fluid-Coated Auxetic PU Foam–Mechanical, Acoustic, And Electromagnetic Properties, J. Intel. Mat. Sys. and Struct., vol. 15, pp. 973–979, 2004.
18. S. Matsuo, M. Tsuruta, M. Hayano, Y. Imamura, Y. Eguchi, T. Tokushima, et al., Phasic Coronary Artery Flow Velocity Determined by Doppler Flowmeter Catheter in Aortic Stenosis and Aortic Regurgitation, The American J. Cardiology, vol. 62, pp. 917–922, 1988.